Hindawi
Journal of Chemistry
Volume 2020, Article ID 7027631, 17 pages
https://doi.org/10.1155/2020/7027631

Research Article

Distribution of Trace Elements, Sr-C Isotopes, and Sedimentary Characteristics as Paleoenvironmental Indicator of the Late Permian Linxi Formation in the Linxi Area, Eastern Inner Mongolia

Linlin Wang,[1] **Yongsheng Zhang**,[2] **Enyuan Xing**,[2] **Yuan Peng**,[2] **and Dongdong Yu**[2]

[1]*Petroleum Exploration & Production Research Institute, SINOPEC, Beijing 100083, China*
[2]*Institute of Mineral Resources, CAGS, Beijing 100037, China*

Correspondence should be addressed to Linlin Wang; wanglinlin.syky@sinopec.com

Received 31 October 2019; Accepted 8 February 2020; Published 7 March 2020

Academic Editor: João Paulo Leal

The Late Permian on the periphery of the Songliao Basin, eastern Inner Mongolia, is an important hydrocarbon source rock system. Its sedimentary environment plays an important role in the evaluation of hydrocarbon prospects in the area. Unfortunately, until now, the interpretation of the sedimentary environment of this area has been controversial. We investigated the Late Permian sedimentary environment by studying the sedimentary characteristics and geochemistry. Based on these investigations, we conclude that the Linxi Formation is mainly composed of clastic sediments, interbedded with limestone lenses, with bioherm limestone at the top of the formation. Inner-layer marine fossils (calcium algae, bryozoans, and sponges) and freshwater and blackish water microfossils (bivalves) are all present, indicative of a typical shallow water sedimentary environment with an open and concussion background. In terms of geochemistry, the formation is relatively light rare Earth enriched, with significant positive Eu anomaly, slight positive La and Y anomaly, weak positive Gd anomaly, and lack of Ce anomaly. The average B/Ga ratio of the mudstone is greater than 3.3, and the average Sr/Ba ratio of the limestone is greater than 1.0. The range of the $^{87}Sr/^{86}Sr$ ratio is from 0.707285 to 0.707953. The range of $\delta^{13}C$ values is from −4.0‰ to 2.4‰. The sediment assemblages, rare Earth elements, trace elements, and $^{87}Sr/^{86}Sr$ and C isotopes of the formation indicate that the Linxi Formation formed in a marine sedimentary environment and occasional marine-terrestrial transitional facies. The formation can be further divided into littoral facies, neritic facies, bathyal facies, and delta front.

1. Introduction

The eastern part of Inner Mongolia in China is located on the junction of the Sino-Korea Plate and the Siberian Plate. During the Permian period, this area experienced an important tectonic transition, and a complex tectonic paleogeographic environment was formed within the sedimentary basin. Since the 20th century, different interpretations have been put forth concerning the paleogeographic environment of the Linxi area of eastern Inner Mongolia during the Late Permian. He et al. interpreted the sedimentary environment of the Linxi Formation, according to the lithology, sedimentary structure, and paleontology of an exposed section in Linxi County. They concluded that the middle-lower parts of the Linxi Formation deposited in the marine environment and the upper part of the Linxi Formation deposited in the terrestrial lake environment [1]. Zhang et al. and Tian et al. concluded that the Linxi Formation formed in a marine sedimentary environment, based on the presence of marine fauna and bioherms in the exposed sections of the Late Permian Linxi Formation in the Linxi area [2, 3]. The other interpretation was that the Late Permian Linxi Formation deposited in terrestrial lake sedimentary environment, according the development of the freshwater bivalve fossils and Angara flora of the Late Permian Linxi Formation in the Linxi area [4–6].

The Late Paleozoic Permian strata in eastern Inner Mongolia are a potential hydrocarbon (oil and gas) resource on the periphery of Songliao Basin. Clarifying the evolution of the sedimentary environment of the strata is important to locate an Upper Paleozoic hydrocarbon generation horizon and predict hydrocarbon prospects in the area. Meanwhile, the lithofacies of the Linxi Formation record the evolution from filling to closing of the Xing-Meng Trough, which is located on the boundary of the Sino-Korea and Siberian Plates. Although previous studies formed some conclusions concerning the Permian sedimentary environment of eastern Inner Mongolia, especially in the Linxi area, some issues still require clarification. This is mainly due to the fact that the fossil types are not consistent throughout the formation and that determining the sedimentary environment of a complete set of formations based on environmentally meaningful typical fossils, sedimentary structures, or bioconstructions has its limitations. This research study investigates the Late Permian Linxi Formation's sedimentary environment, by analyzing the sedimentary characteristics and the geochemical characteristics of the Linxi Formation in the Linxi area, eastern Inner Mongolia.

2. Regional Geological Survey

2.1. Structure Distribution. The eastern part of Inner Mongolia is located in the Xing-meng orogenic zone. It is bordered in the west and north by the Mongolia-Okhotsk suture zone, which is adjacent to Mongolia and Russia. In the south, it is bordered by the Xar Moron River-Yanji suture zone, which is adjacent to the North China plate. In the east, it is bordered by the Central Sikhote subduction belt near the Pacific Plate. The Linxi area is located east of the Xing-meng orogenic belt and north of the Xar Moron River fault in the area where the Sino-Korea and Siberian Plates meet (Figure 1(a)). The Linxi Formation is mainly distributed in the Keshiketeng Banner and Linxi County. It is an important Permian lithostratigraphic unit in the Upper Permian strata of eastern Xing-meng. The underlying Middle Permian Wujiatun Formation is composed of marine carbonates, volcanic rocks, and clastic sediment, and the overlaying Lower Triassic Xingfulu Formation is composed of terrestrial clastic sediments [7].

2.2. Lithologic Characteristics. The Late Permian Linxi Formation can be divided into 5 sections, which we call sections Lin1-5. Section Lin1 is composed of medium-thick gray and gray-green medium-fine-grained sandstone, thin-bedded siltstone, and interbedded siltstone (A1 and A2 in Figure 2), which is locally interbedded with thin-medium calcarenite or limestone lenses. Section Lin2 is composed of dark gray, grayish-black shale, silty mudstone, and silty slate interbedded with gray-green fine sandstone, and it locally contains visible slump breccia and limestone lenses (A3 and A4 in Figure 2). Section Lin3 is composed of medium-thick light brown medium-coarse grained sandstone interbedded with thin gray, gray-brown siltstone, argillaceous siltstone, and silty mudstone and local areas of medium-thick gravel coarse grained sandstone and limestone (A5 in Figure 2). The entire section from bottom to top evolved from sandstone and pebbled sandstone to middle-thick sandstone and upper interbedded sandstone and mudstone. Section Lin4 is composed of dark gray, gray-black shale, silty mudstone, and argillaceous siltstones interbedded with thick gray-green, gray fine grained sandstone, thin-medium limestone, and limestone lenses (A6 and A7 in Figure 2). The lower part of this section is primarily composed of argillaceous siltstone and silty mudstone. The middle part of the section is dominated by shale, while the upper part of the section is composed of interbedded sandstone and mudstone interbedded with limestone lenses. Section Lin5 is composed of gray argillaceous siltstone, sandy mudstone, light gray medium-fine grained sandstone, tuffaceous sandstone, massive gray bioherm limestone, and framestone (A8 in Figure 2).

2.3. Sedimentary Structures and Paleontology Fossils. The Linxi Formation contains many types of sedimentary structures and paleontology fossils. In the lower part of section Lin1, wedge-shaped cross bedding, tabular cross bedding, and symmetrical ripple bedding are present in the sandstones, while horizontal bedding (B1 in Figure 2), current bedding, and small-scale cross bedding are present in the mudstone-siltstones and argillaceous siltstones. The upper part of section Lin1 sandstones contain parallel bedding, oblique bedding, small-scale cross bedding, and current bedding (B2 in Figure 2), indicating a shallow water concussion environment, containing bivalves *Palaeanodonta* sp., *Palaeomutella* sp., *Anthraconaia* sp., and fragments of plant fossils. The lower part of section Lin2 contains wash-out structures (B3 in Figure 2), locally developed slump structures, deformation bedding (B4 in Figure 2), and small current bedding, indicating a relatively deep-water environment. The imbricated structure observed in the lower part of section Lin3 exhibits parallel bedding and tabular cross bedding (B6 in Figure 2) in the sandstones and current bedding, concussion ripples, bioturbation structures (B5 in Figure 2), and mud cracks in the mudstones (B7 in Figure 2), which is indicative of an intermittently exposed shallow water environment. The middle and upper parts of section Lin3 exhibit lenticular foreset bedding and local contemporaneous slump structures and contain bivalve fossils (*Palaeodoronella soronensis*, *Palaeodonta* sp., *P.* cf. *trigonalis*, *P.* cf. *semilunulata*, and *P. hahaiensis*) and plant fossil debris, which is indicative of a delta front sedimentary environment. In section Lin4, low angle oblique bedding, graded bedding, concretionary structure (B8 in Figure 2), and small-scale ripple bedding developed can be seen. The clastic rocks of section Lin4 contain conchostracas (*Huanghestheria* sp., *Palaeolimnadia* sp., and *Pemphicyclus* cf. *trochoides*), bivalve fossils (*Palaeanodonta* sp., *P.* cf. *trigonalis*, and *Palaeomutela soronensis*), plant fragments, and brachiopod fossil fragments. Bryozoans, sponges, and calcareous fossils, including *Monostysisyrinx* gen. and *Archaeolithoporella* gen., can be seen in the limestone, indicating an expansive coastal environment that may have

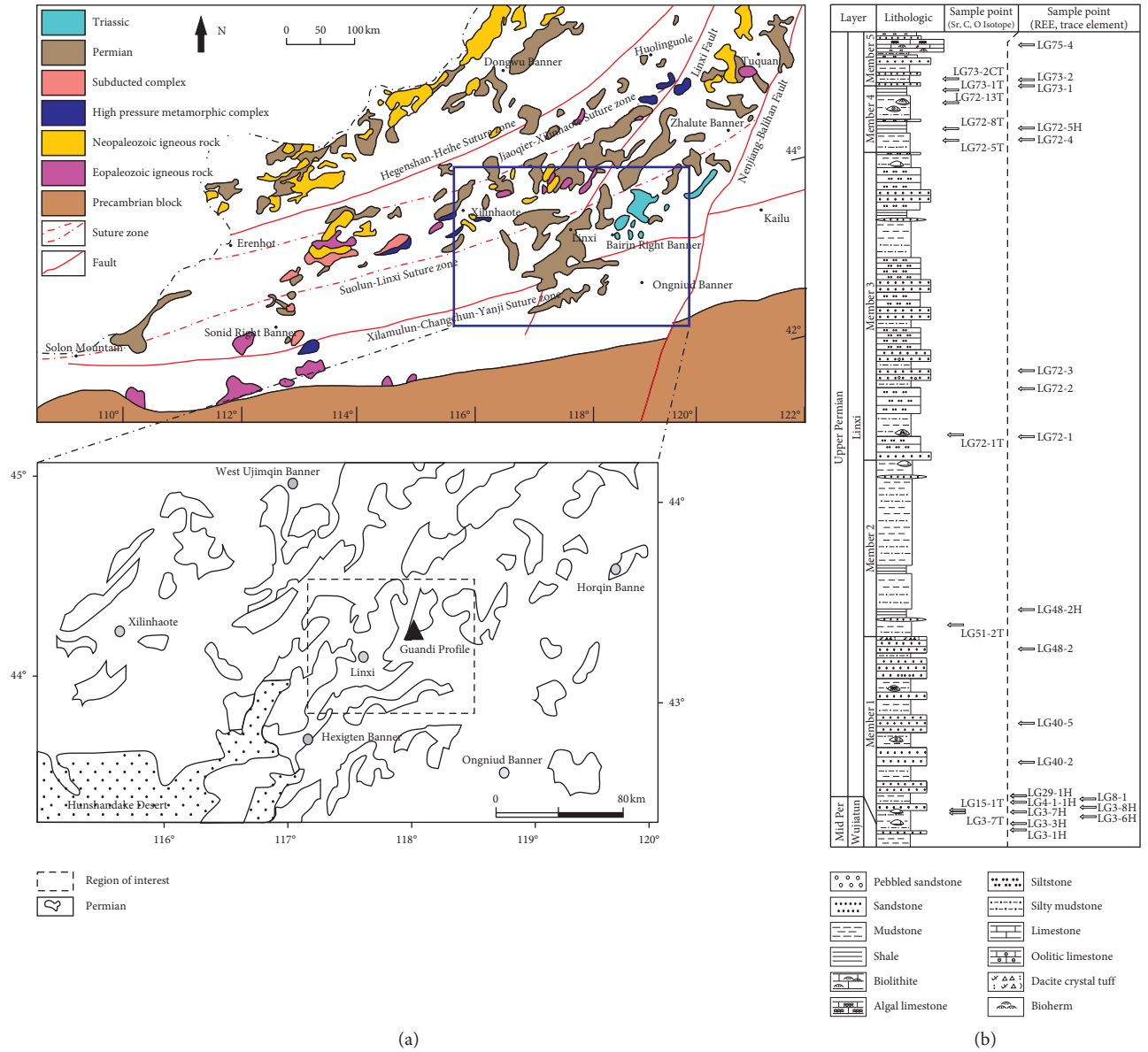

FIGURE 1: Tectonics and stratigraphy of eastern Inner Mongolia: (a) tectonic belt, stratum plane distribution, and the location of Guandi profile in the Linxi area; (b) the lithological section and sample distribution of Linxi Formation.

mixed a terrestrial source. The lower part of section Lin5 exhibits wedge-shaped cross bedding and parallel bedding, while the middle and upper parts exhibit visible bioturbation structures, concretionary structures, low angle oblique bedding, and small-scale cross bedding. Bryozoans and sponge bone fossils are present in the limestone [7], indicating a neritic environment.

3. Samples and Analytical Procedures

The strata discussed in this paper and the samples used for geochemical analysis were primarily collected from the Guandi profile in Linxi County in eastern Inner Mongolia (Figure 1(b)). A total of 33 samples were analyzed. All the samples are fresh and uncontaminated rocks by stripping a weathered layer. Observed under the microscope, the samples were without epigenic dikes or strong recrystallization. Of these samples, 4 of them were limestone of Early Triassic, which were analyzed for Sr-C isotopic ratios. 24 of the samples were primarily composed of lenticular limestones from the Linxi Formation. They were analyzed for major, trace, and rare Earth elements and Sr-C isotopic ratios (Tables 1–3). Seven of the samples were mudstone, which were analyzed for major, trace, and rare Earth elements (REEs) (Table 1). The X-ray fluorescence spectroscopy (XRF) was used to determine the oxides of major elements. The LOI (loss on ignition) of the samples was recorded as weight loss after burning at 1000°C. Trace and rare Earth elements were determined by an Element 6000 inductively-coupled plasma mass spectrometer (ICP-MS). Both of the

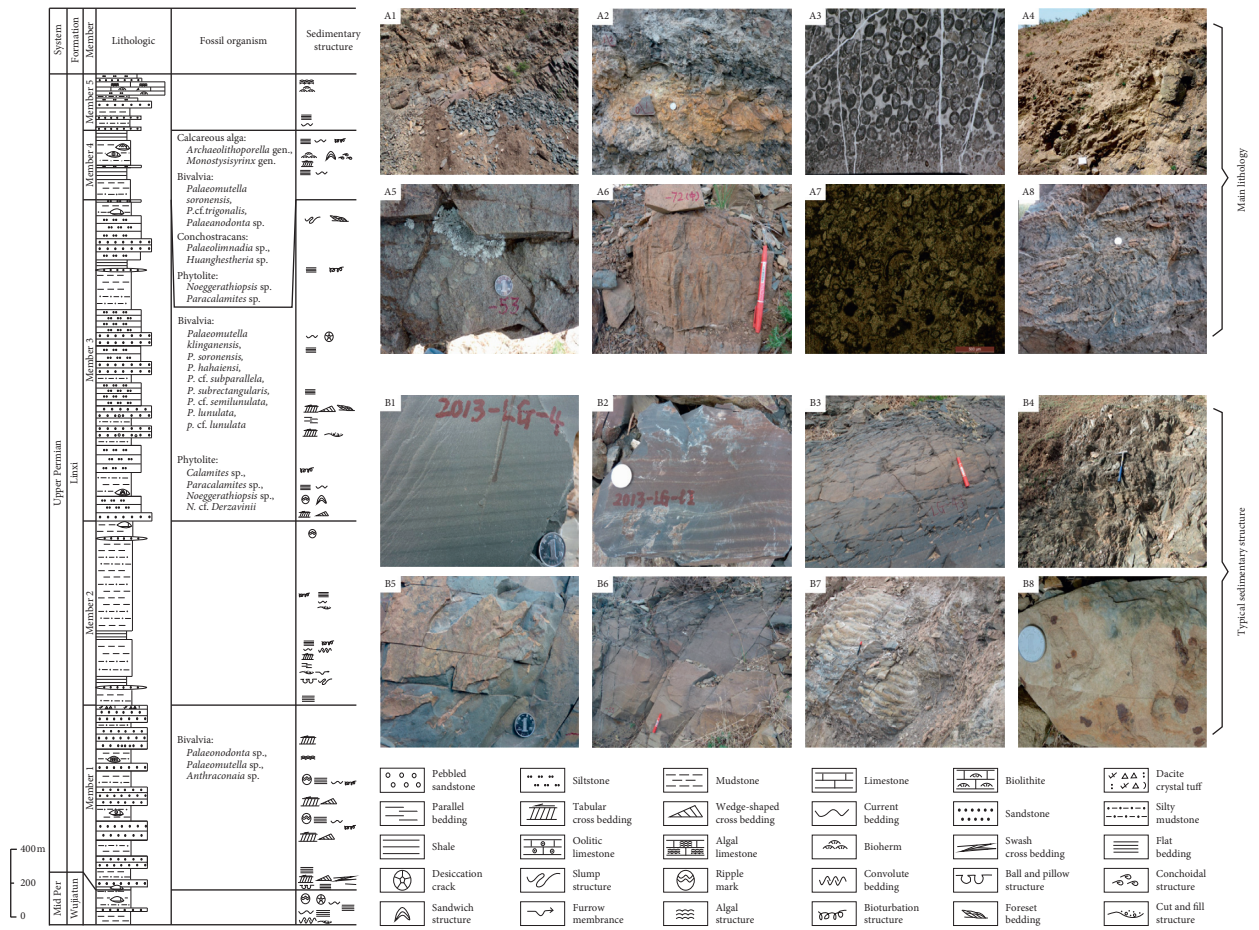

Figure 2: Sedimentary characteristics of the Late Permian Linxi Formation in the Linxi area of eastern Inner Mongolia. A1, gray mudstone, section Lin1. A2, gray silty mudstone interbedded with thin yellowish brown silty mudstone, section Lin1. A3, oolitic limestone, light crystal matrix, containing a small amount of oolitic spherulites. A4, slump conglomerate, indicating gravity flow, section Lin2. A5, gray gravel coarse grained sandstone, gravel size 0.2–1.0 cm, subround and subangular gravel that is mainly limestone, section Lin3. A6, laminated limestone with laminated columnar structures, section Lin4. A7, inner clastic granular limestone, particles are mainly inner debris, algae grains, and ooids, section Lin4. A8, framestone with an algae bonding structure, section Lin 5. B1, gray-green silty mudstone with horizontal bedding, section Lin1. B2, gray siltstone with current bedding, section Lin1. B3, lower dark gray mudstone with wash-out structures, unconformably in contact with upper gray sandstone, section Lin 2. B4, gray sandy mudstone with slump and deformation structures, section Lin3. B5, dark gray fine grained sandstone with bioturbation structures, section Lin3. B6, gray fine grained sandstone with tabular cross bedding, section Lin3. B7, gray argillaceous sandstone with ripple bedding and mud cracks, section Lin3. B8, light brown coarse grained gravel sandstone with concretionary structures, section Lin4.

tests were performed in the Chinese Academy of Geological Sciences National Geological Experimental Testing Center following the method described by Ryu et al. [15]. The Sr isotopes were analyzed using a British VG354 isotope mass spectrometer following the method described at the Nanjing Institute of Soil Science and Technology Service Center, Chinese Academy of Sciences. The measured value of $^{87}Sr/^{86}Sr$ for American isotope standard NBS987Sr was 0.710236 ± 7 ($n = 10$) with a precision of ±0.005%. The C isotopes were analyzed using MAT-252 isotope mass spectrometer with a precision of ±0.2‰ at Isotope Research Laboratory, Institute of Mineral Resources, Chinese Academy of Geological Sciences.

4. Results

4.1. Rare Earth Elements and Trace Elements. Trace element concentrations are reported in Table 1. REE + Y concentrations were normalized to the Post-Archaean Australian Shale (PAAS) composite [16]. The total REE content (ΣREE) of the sediments in the Linxi Formation ranges from 10.07 μg/g to 195.69 μg/g with an average of 76.56 μg/g. These samples of mudstones and lime mudstones with high REE are clearly contaminated by a considerable terrigenous debris component and perhaps masking the anomalies distribution of REE in marine environments. Thus, they are not used any further for palaeoenvironmental reconstructions.

Table 1: The trace element concentration (in ug/g) of the Linxi Formation in the Guandi profile.

Number	LG 3-1H	LG 3-3H	LG 3-6H	LG 3-7H	LG 3-8H	LG 4-1-1H	LG 8-1	LG 29-1H	LG 40-2	LG 40-5	LG 48-2	LG 48-2H	LG 72-1	LG 72-2	LG 72-3	LG 72-4	LG 72-5H	LG 73-1	LG 73-2	LG 75-4
Lithology	Limestone	Limestone	Mudstone	Limestone	Lime mudstone	Mudstone	Bioclastic limestone	Mudstone	Bioclastic limestone	Bioclastic limestone	Lime mudstone	Lime mudstone	Bioclastic limestone	Bioclastic limestone	Bioclastic limestone	Bioclastic limestone	Bioclastic limestone	Bioclastic limestone	Bioclastic limestone	Mudstone
B	18.5	18	94.7	11.5	150	95.7	16.6	57.3	8.34	15.1	33.4	46.7	6.4	14.2	10.8	8.37	13.6	10	3.45	38.1
Ga	4.34	5.28	20.5	3.82	18.9	22.1	6.57	17.1	3.96	0.52	8.1	7.7	1.91	3.15	3.67	3.43	4.35	2.58	0.68	20.1
Rb	27.9	22.4	143	19.7	197	153	39	122	10.7	14.8	41.7	55.6	14.4	24.7	26.9	16.2	15.4	20.8	3.34	116
Sr	1193	950	82.7	1259	351	131	917	58.9	1172	486	692	626	1164	1449	1059	1465	871	1140	3052	250
Ba	166	157	442	70.6	519	461	109	591	49.5	22.2	224	355	86.2	150	204	133	129	95.1	219	581
La	5.39	5.85	33.7	3.38	29.6	37.3	8.14	38.4	7.37	1.95	15.1	14.3	8.96	9.12	7.44	13.4	18.1	7.38	3.74	34.9
Ce	11.8	12.1	70.2	7.3	62.3	77.2	15.9	78.5	15.9	4.06	31.7	25.3	15.4	16	14.3	22.3	35.7	14.1	8.13	60.1
Pr	1.37	1.31	8.15	0.78	7.2	8.98	1.92	9.35	1.96	0.4	3.81	2.99	1.69	1.87	1.51	2.48	4.12	1.52	0.97	7.2
Nd	5.44	5.13	32.2	3.24	26.9	35.7	7.68	37.3	8.42	1.73	15.4	12.6	6.77	8	6.29	9.8	17.1	6.33	4.86	28.1
Sm	1.21	1.16	6.39	0.68	5	7.2	1.55	7.25	2.11	0.37	3.4	2.72	1.54	1.75	1.33	2.18	3.43	1.48	1.41	5.91
Eu	0.43	0.91	1.19	0.31	1.45	1.26	0.53	1.35	0.85	0.13	1.07	0.97	0.54	0.83	0.48	0.74	0.76	0.54	0.73	1.26
Gd	1.29	1.17	6	0.78	5.1	7.17	1.49	6.79	2.41	0.37	3.76	2.83	1.78	1.97	1.39	2.57	3.41	1.68	1.82	5.75
Tb	0.2	0.19	0.97	0.12	0.85	1.09	0.23	1.08	0.38	0.06	0.64	0.44	0.28	0.29	0.21	0.39	0.57	0.26	0.25	0.84
Dy	1.1	0.98	5.61	0.7	4.99	6.1	1.38	5.96	2.22	0.37	3.62	2.75	1.75	1.64	1.33	2.45	3.2	1.6	1.41	5.24
Ho	0.23	0.19	1.15	0.14	1.04	1.24	0.28	1.27	0.45	0.08	0.77	0.58	0.38	0.33	0.27	0.51	0.66	0.35	0.26	1.11
Er	0.65	0.58	3.21	0.41	2.82	3.51	0.81	3.7	1.19	0.24	2.08	1.68	1.09	0.89	0.86	1.57	1.91	1.01	0.67	3.12
Tm	0.09	0.08	0.45	0.05	0.42	0.52	0.13	0.55	0.16	0.03	0.32	0.27	0.16	0.12	0.13	0.23	0.28	0.15	0.09	0.47
Yb	0.6	0.52	3.04	0.36	2.58	3.37	0.8	3.64	1.06	0.26	2.13	1.82	1	0.74	0.83	1.47	1.72	0.92	0.58	3.06
Lu	0.1	0.08	0.49	0.06	0.39	0.5	0.13	0.55	0.15	0.02	0.33	0.26	0.15	0.11	0.12	0.23	0.26	0.13	0.08	0.46
ΣREE	29.90	30.25	172.75	18.3	150.64	191.14	40.97	195.69	44.63	10.07	84.13	69.51	41.49	43.66	36.49	60.32	91.22	37.45	25.00	157.52
LREE	25.64	26.46	151.83	15.69	132.45	167.64	35.72	172.15	36.61	8.64	70.48	58.88	34.90	37.57	31.35	50.90	79.21	31.35	19.84	137.47
HREE	4.26	3.79	20.92	2.62	18.19	23.50	5.25	23.54	8.02	1.43	13.65	10.63	6.59	6.09	5.14	9.42	12.01	6.10	5.16	20.05
La_{SN}/Yb_{SN}	0.66	0.83	0.82	0.69	0.85	0.82	0.75	0.78	0.51	0.55	0.52	0.58	0.66	0.91	0.66	0.67	0.78	0.59	0.48	0.84
(La/La*)	1.03	1.13	1.07	1.28	0.94	1.09	1.13	1.09	1.23	1.63	1.09	1.47	1.42	1.57	1.47	1.40	1.29	1.44	2.73	1.22
(Ce/Ce*)	1.00	1.01	0.98	1.04	0.98	0.97	0.93	0.96	0.96	1.06	0.96	0.89	0.91	0.89	0.98	0.89	0.95	0.97	0.98	0.87
(Eu/Eu*)	1.61	3.66	0.90	1.98	1.35	0.82	1.64	0.90	1.75	1.65	1.40	1.64	1.52	2.08	1.65	1.45	1.04	1.59	2.10	1.02
(Gd/Gd*)	0.98	0.89	0.98	1.04	0.97	1.02	1.07	0.96	1.02	1.05	0.92	1.11	1.09	1.06	1.15	1.14	0.93	1.09	1.13	1.17
Y/Ho	26.61	31.53	24.87	25.29	24.33	25.00	31.54	24.72	30.89	34.38	25.32	28.97	37.11	36.06	34.15	33.73	27.88	35.43	38.46	27.21

La_{SN}/Yb_{SN} is the ratio of La and Yb by PAAS normalized.

We mainly use the trace elements of the carbonates and argillaceous carbonates to discuss the palaeosedimentary environment of the Linxi Formation. Shale-normalised (SN) elemental anomalies were calculated on a linear scale, assuming that differences in concentration between neighbouring pairs are constant, as follows: $La/La^* = La/(3Pr - 2Nd)_{PAAS}$, $Ce/Ce^* = Ce/(0.5La + 0.5Pr)_{PAAS}$, $Eu/Eu^* = Eu/(0.5Sm + 0.5Gd)_{PAAS}$, and $Gd/Gd^* = Gd/(2Tb - Dy)_{PAAS}$.

The ΣREEs of the limestones are between 10.07 μg/g and 91.22 μg/g. Abbreviations are applied to light REE (LREE) and heavy REE (HREE). As can be seen from the PAAS normalized REE distribution pattern (Figure 3(a) and Table 1), the limestone samples of Linxi Formation in the Guandi profile of Linxi area display relatively uniform shale-normalised REE + Y patterns (Figure 3(a)). The LREE depleted relative to the HREE with La_{SN}/Yb_{SN} from 0.48 to 0.91, and the limestones display a significant positive Eu anomaly ($(Eu/Eu^*)_{SN} = 1.78$). But significant differences can be noted between the limestones at the bottom of Lin1 and the other limestones of Linxi Formation. The limestones at the bottom of Lin1 show a slight positive La anomaly ($(La/La^*)_{SN} = 1.16$), lack of Ce, Gd, and Y anomaly ($(Ce/Ce^*)_{SN} = 0.99$), ($(Gd/Gd^*)_{SN} = 1.0$), and ($(Y/Ho)_{SN} = 1.07$). The other limestones of Lin1-5 show a distinct positive La anomaly ($(La/La^*)_{SN} = 1.6$), slight positive Y anomaly ($(Y/Ho)_{SN} = 1.25$), weak positive Gd anomaly ($(Gd/Gd^*)_{SN} = 1.08$), weak negative Ce anomaly ($(Ce/Ce^*)_{SN} = 0.93$, except sample LG 40-2), and lack of Ce anomaly ($(Ce/Ce^*)_{SN} = 0.95$) (Table 1).

In addition to REE analysis, other trace element (Sr, Ba, B, and Ga) analyses were conducted on the limestones and mudstones from the Guandi profile in the Linxi area (Table 1). In the Linxi Formation, the Sr content ranges from 58.9 μg/g to 3052 μg/g with an average of 918.43 μg/g. The Ba content ranges from 22.2 μg/g to 591 μg/g with an average of 238.18 μg/g. The Sr/Ba ratios of the limestone range from 1.76 to 23.68 with an average of 8.18. The B content of the mudstones ranges from 18 μg/g to 150 μg/g with an average of 57.21 μg/g, which is enriched compared to the average B content of the crust (7.6 μg/g). The Ga content ranges from 4.34 μg/g to 22.1 μg/g with an average of 12.95 μg/g. The B/Ga ratios of the mudstone range from 1.90 to 7.94 with an average of 4.42.

4.2. Sr and C Isotope Distribution. The whole rock total Sr content and Sr isotopic data for the Linlin Formation in the Linxi area are presented in Table 2. The C isotopic data for the Linlin Formation are presented in Table 3. The results show that the Sr contents of all nine limestone samples in the Linxi Formation are greater than 850.0 μg/g with a maximum value of 2762.0 μg/g and an average of 1435.1 μg/g. The $^{87}Sr/^{86}Sr$ values of the limestone samples range from 0.707285 to 0.707953 with an average of 0.707624. The $\delta^{13}C$ values of the limestone samples vary from −4.0‰ to 2.4‰, and the average is −1.3‰. As shown in Figure 4, there is no correlation between Sr-C isotope and Mn/Sr, and the Mn/Sr ratio reaches the upper limit of 2-3 for qualified samples recommended by Kaufman et al. [27]. Seven samples have low Mg/Ca ratios (<0.1) and may be presumed to be unaltered. The Sr contents of all of the limestone samples are significantly larger than the minimum Sr content (400 μg/g) suggested by Korte et al. in their Sr isotope deposition studies [28]. In addition, there is no correlation between $^{87}Sr/^{86}Sr$ and Si (representing SiO_2 content) (Figure 4(b)), indicating that the Sr isotopic composition is completely derived from the endogenous sedimentary limestone and is not affected by other Si-bearing terrestrial debris and smaller diagenesis events. This indicates that the Sr–C isotopes in the limestone represent the Sr-C isotopes of the sedimentary fluids.

5. Discussion

5.1. REE Distribution and Sedimentary Environment. The REEs of different water bodies are quite different. The chemical composition of the authigenic minerals and rocks formed by these water bodies can be used to determine the geochemical characteristics of modern and ancient sedimentary media [29–32]. The water involved in the formation of carbonate rocks mainly fall into three categories: seawater, rivers or atmospheric precipitation, and hydrothermal fluid. The behavior of REE in a given type of water body results in distinguishing characteristics. In seawater, the LREE is being depleted relative to the HREE and results in La enrichment [17]. In addition, the REE of seawater in oxygen environment is resulting in Ce depletion [33]. In rivers, lakes, and other freshwater medium, Ce usually exhibits a slight anomaly or no anomaly. The infiltration of weathered leaching water near Eu-rich rocks or Eu bonded to iron hydroxide in water also causes slight positive Eu anomalies [22]. Beyond that, an influx of high-temperature midocean ridge oceanic hydrothermal fluids can also cause positive Eu anomalies.

In order to facilitate a more direct comparison of the REE contents of the different water bodies, PAAS was used to normalize the REE of the ancient marine carbonates and minerals, modern seawater, lakes, lacustrine carbonate rocks, and hydrothermal fluids [17, 18, 20–25] (Figures 3(b)–3(h)). Among the rare Earth patterns of the different sediments, water, and minerals, normal seawater has enriched La, negative Ce anomalies, and slightly enriched Gd (Figures 3(b) and 3(c)). The hydrothermal fluids from the median ridge have obvious positive Eu anomalies (Figure 3(g)). The freshwater and the lacustrine carbonate rocks are characterized by a relatively flat REE patterns without obvious anomaly distribution (Figures 3(e) and 3(h)). The gulf and coastal waters have positive Ce anomalies and small negative Eu anomalies and show relatively gentle HREE distribution patterns (Figure 3(d)). The marine carbonate rocks and minerals have enriched La, small negative Ce anomalies, and positive Eu anomalies (Figure 3(f)). The samples from a distal section of near-shore marine carbonates display a distinct positive Y anomaly, positive La anomaly, and slight positive Gd anomaly. In contrast, the samples from the proximal section of near-shore marine carbonates display a slight positive Y anomaly,

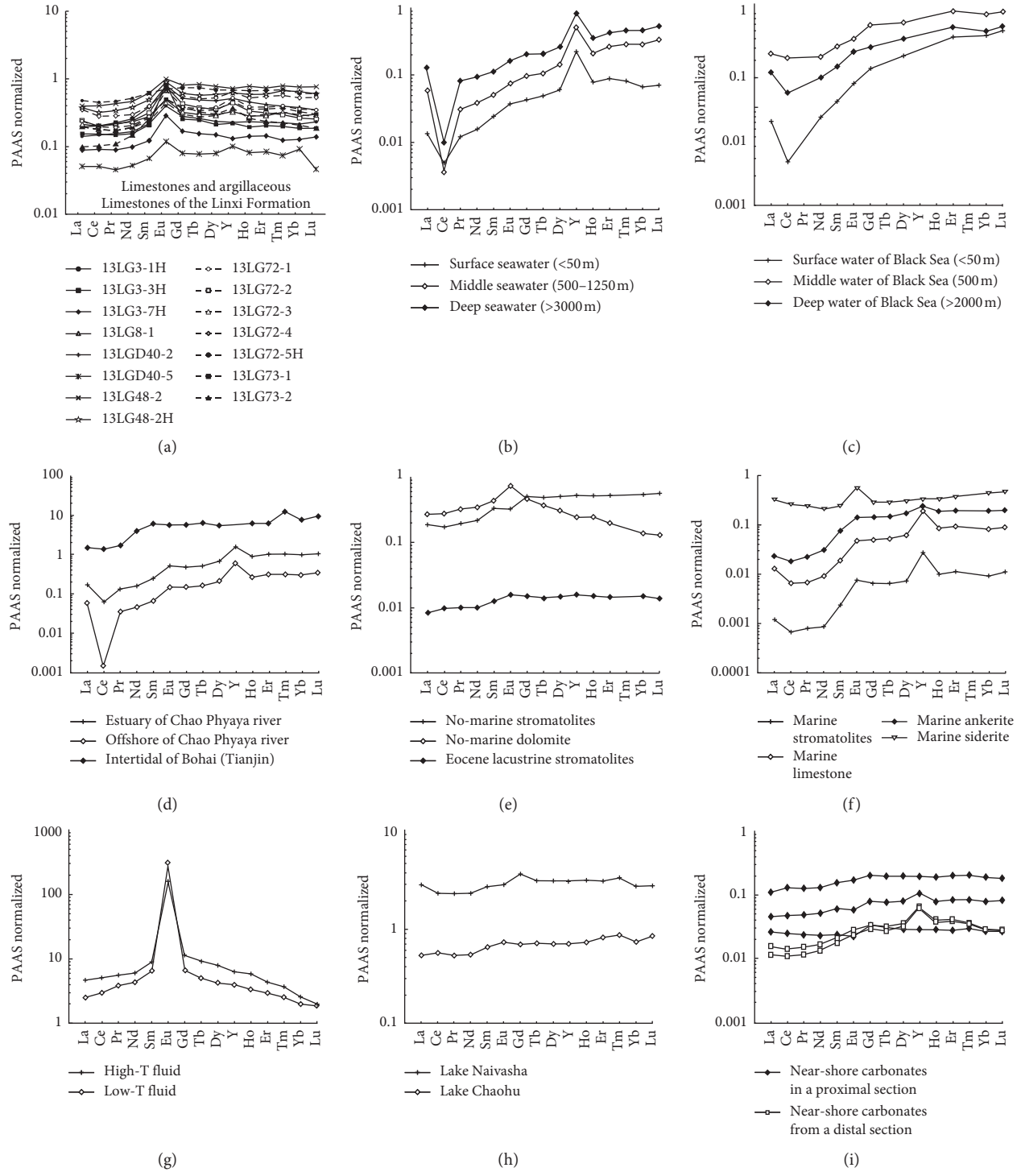

Figure 3: PAAS standardized comparison chart of the REEs of the Linxi area Guandi profile sediments and the REE of other water bodies, rocks, and minerals: the REEs of (a) limestone and mudstone in Linxi Formation, (b) seawater from southwestern Pacific [17], (c) seawater in an oxygen-poor environment of the Black Sea [18], (d) the Chao Phraya River estuarine area and distant end [19], seawater form intertidal of Bohai Sea [20], (e) nonmarine carbonate rocks [21], (f) marine carbonate rocks and marine carbonate minerals [22], (g) the high-T and low-T marine hydrothermal fluids form mid-Atlantic ridge [23], (h) water from Lake Naivasha and Chaohu Lake [24, 25], and (i) near-shore carbonates of the Bloeddrif Member, lower Holgat Formation from a proximal section south of the Kuboos Pluton, and a distal section north of the Kuboos Pluton [26].

weak positive Gd anomaly, and a lack of La anomaly (Figure 3(i)). It can be noted by the distribution characteristics of REE, except of the Eu, the limestones of Linxi Formation in the Guandi profile of Linxi area display relatively uniform shale-normalised REE + Y patterns (Figure 3(a)). The limestones at the bottom of Lin1 display a

Table 2: Sr isotope values of the limestone from the Linxi area Guandi profile and compared with other parts of the world.

$^{87}Sr/^{86}Sr$ (Linxi Formation of Permian in Linxi area, Inner Mongolia)									
Number	LG3-7T	LG15-1T	LG51-2T	LG72-1T	LG72-5T	LG72-8T	LG72-13T	LG73-1T	LG73-2CT
Lithology	Limestone	Oomicrite	Stromatolitic limestone	Limestone	Bioclastic limestone	Bioclastic limestone	Stromatolitic limestone	Limestone	Bioclastic limestone
SiO_2 (%)	13.61	3.11	14.02	18.76	18.48	12.9	11.05	8.93	13.61
MnO (%)	0.30	0.51	0.30	0.23	0.21	0.42	0.51	0.28	0.30
Sr(ug/g)	1275	1639	1604	930.7	859.5	1123	1225	1498	2762
$^{87}Sr/^{86}Sr$	0.707719	0.707593	0.707684	0.707526	0.707758	0.707953	0.707297	0.707802	0.707285
$^{87}Sr/^{86}Sr$ (lacustrine carbonate rocks of Triassic in Linxi area, Inner Mongolia)									
Number	BLS-1	BLS-2	BLS-3	BLS-4					
$^{87}Sr/^{86}Sr$	0.713605	0.714335	0.711949	0.714164					
$^{87}Sr/^{86}Sr$ (marine carbonate and conodonts of Permian/Triassic in the other places of the world)									
Marine limestone of Permian in South China[1]	0.70732	0.70757	0.7076	0.70754	0.70753	0.70757	0.70734	0.70744	0.70744
	0.70741	0.70744	0.70742	0.70745	0.70739	0.70740	0.70749	0.70747	0.70750
	0.70757	0.70758	0.70748	0.70752	0.70755	0.70722	0.70739	0.70767	
Conodonts from Permian/Triassic boundary in Abadeh, Iran[2]	0.707038	0.707079	0.707092	0.707218	0.707225	0.707219	0.707266	0.707392	0.70739
	0.706923	0.706970	0.707010	0.707006	0.70699	0.706945	0.707050	0.707138	0.707046
Marine carbonate of late Permian in upper Yangtze region[3]	0.70743	0.70742	0.70684	0.70697	0.70722	0.70672	0.70755	0.70725	0.70752
Conodonts of Permian/ Triassic, United States[4]	0.708111	0.708132	0.708878	0.708841	0.707957	0.708011	0.708093	0.708345	0.707605
	0.707453	0.707629	0.707643	0.707561	0.707506	0.707513	0.707416	0.707461	0.707336
	0.707341	0.707333	0.707388	0.707331	0.707229	0.706914	0.707031	0.706948	0.707247
	0.707406	0.707059	0.707027	0.706913	0.70734	0.707404	0.707373	0.707133	0.707208
	0.707406	0.707059	0.707027	0.706913	0.70734	0.707404	0.707373	0.707133	0.707208
Conodonts of Permian/ Triassic, Pakistan[5]	0.707211	0.707388	0.707117	0.70719	0.707168	0.707200	0.707100	0.707102	0.707117
	0.707186	0.707240	0.707130	0.707399	0.707690	0.707322	0.707427	0.707736	0.707499
	0.707568	0.707458	0.707587	0.707469	0.707440	0.707503	0.707308	0.707626	0.707856

[*1]Data from Tian and Zheng [8]; [*2]data come Korte et al. [9, 10]; [*3]data come Huang et al. [11]; [*4,*5]data from Martin and Macdougall [12].

Table 3: Carbon isotopic data of Permian-Early Triassic carbonate rocks in Linxi area and other regions.

C isotope (Linxi Formation of Permian in Linxi area, Inner Mongolia, China)									
Sample number	LG3-7T	LG15-1T	LG51-2T	LG72-1T	LG72-5T	LG72-8T	LG72-13T	LG73-1T	LG73-2CT
$\delta^{13}C$	−4.0	−0.3	−0.4	0.1	2.4	−3.3	−3.2	−0.2	−2.6
C isotope (lacustrine carbonate of Triassic in Linxi area, Inner Mongolia, China)									
Sample number	BLS-2	BLS-3	BLS-4	BLS-5	BLS-6	BLS-7	BLS-8	BLS-9	BLS-11
$\delta^{13}C$	−6.5	−7.4	−9.4	−8.6	−11.0	−9.9	−8.7	−11.4	−8.5
[*1]C isotope (marine limestone of Permian and lacustrine limestone of Triassic, Inner Mongolia, China)									
$\delta^{13}C$	P_2	−1.15	−0.71	−2.89	T_1	−6.22	−6.22	−12.41	−4.18
[*2]C isotope (marine carbonate of Permian in Khorat basin, Thailand)									
$\delta^{13}C$	2.06	3.77	4.17	3.01	3.12	2.75	0.88	4.52	−2.78
[*3]C isotope (marine limestone of the Changhsingian late Permian, Changxing, Zhejiang, China)									
$\delta^{13}C$	−3.0	0.0	−0.4	−0.3	1.0	0.9	3.7	1.9	3.9
	2.3	3.3	3.8	0.5	1.6	2.9	−0.2	2.2	2.8
	−2.5	−1.9	1.7	1.5	1.5	1.9	1.5	2.3	1.9
	2.8	2.7	1.4	2.1	2.0	2.4	2.2	1.6	−1.3
	−3.4	1.8	1.8	2.0	2.5	2.2	1.8	0.5	−3.0

[*1]Data from He et al. [1]; [*2]data from Du et al. [13]; [*3]data from Li. [14].

slight positive La anomaly and lack of Ce, Gd, and Y anomaly, which are closed to the REE distribution patterns of lake water, no-marine carbonates, and the proximal section of near-shore marine carbonates (Figures 3(e), 3(h), and 3(i) and 5). The middle-upper limestone samples of Lin1 and the limestones of Lin2-5 display a distinct positive La

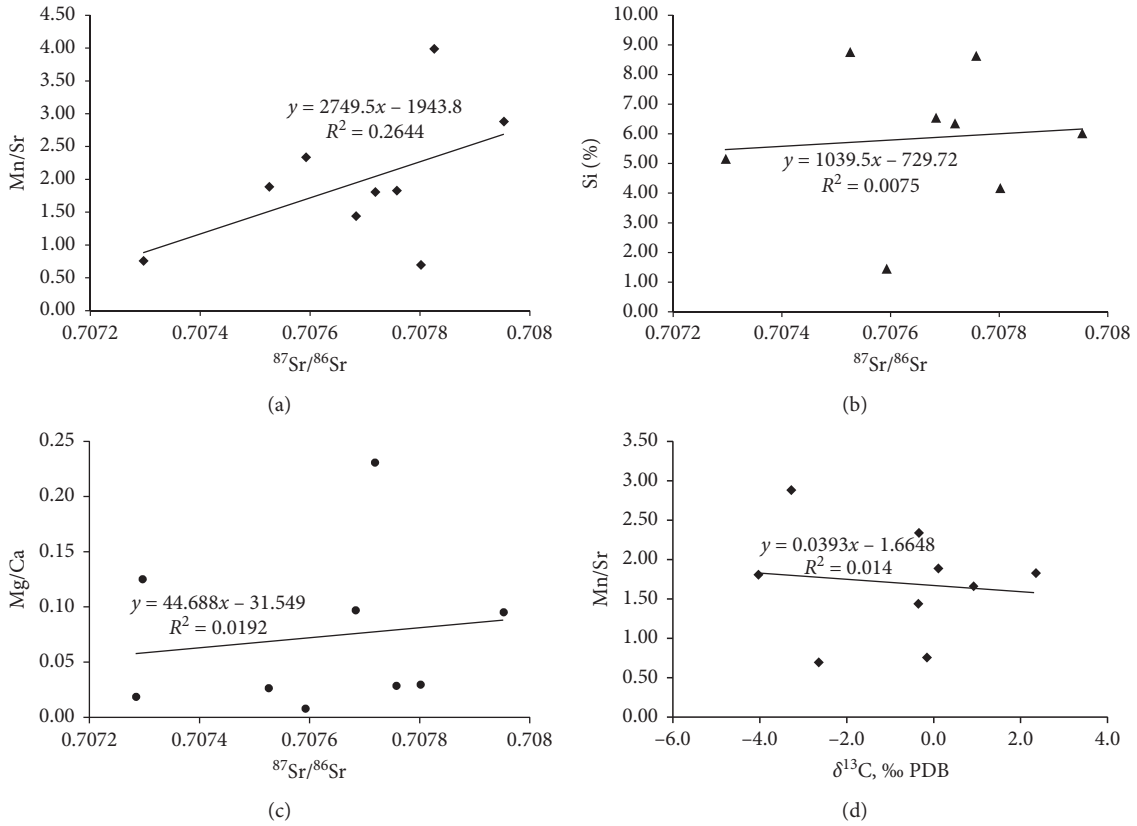

Figure 4: The relationship to distinguishing the diagenesis of the Linxi Formation samples: (a) relationship between the $^{87}Sr/^{86}Sr$ values and Mn/Sr values; (b) relationship between the $^{87}Sr/^{86}Sr$ values and Si contents; (c) relationship between the $^{87}Sr/^{86}Sr$ values and Mg/Ca values; (d) relationship between the $\delta^{13}C$ values and Mn/Sr ratios.

anomaly, slight positive Y anomaly, weak positive Gd anomaly, and lack of Ce anomaly, and its REE patterns resemble those deposits from the distal section of littoral environments, which is dominated by the ocean but with freshwater inputs from continental weathering (Figures 3(f) and 3(i)) or the neritic environments with a terrestrial source mixing. In addition to the above REE of La, Ce, Gd, and Y, almost all the limestones of the Linxi Formation display a distinct positive Eu anomaly. The Eu positive anomalies have no obvious indication of the sedimentary environment. With the lack of Eu positive anomaly in mudstones and no obvious correlation between the concentration of Eu and iron oxide (not shown), we infer that the reason for the positive Eu anomaly is related to the hydrothermal fluid mixing.

5.2. Trace Element Distribution and Sedimentary Environment. In addition to REE, other trace element ratios of sedimentary rocks can also be used to determine their sedimentary environments. The Sr in fine-grained marine sediments tends to be enriched relative to Ba, causing the higher Sr/Ba value in the fine-grained sediments. Therefore, the relative contents of Sr and Ba recorded by the fine-grained sediments, especially in mudstones and shales, i.e., Sr/Ba, are positively correlated with the paleosalinity [34–36]. Wei and Algeo conducted a comprehensive study of the Sr/Ba ratios as paleosalinity proxies in ancient shales and mudrocks, and they concluded that the Sr/Ba ratio of freshwater is less than 0.2, the Sr/Ba ratio from 0.2 to 0.5 indicate brackish environments, and ratios greater than 0.5 represent the marine environments. When water depth increases in sedimentary basins, the energy of seawater decreases with the increased clay minerals and fine-grained material. The fine-grained sediment enhances the adsorption of Ba ions and causes a lower Sr/Ba ratio. In general, the Sr/Ba ratios is lower in deep sea or bathyal sediments [36]. In addition, the incorporation of terrigenous debris in the offshore area can also result in a decrease in Sr/Ba ratios of argillaceous sediments. We compared the Sr and Ba contents of the Permian sedimentary rocks in the other areas of China (Figure 6 and Table 4) [34, 37, 38]. The Sr/Ba ratios of the marine mudstones of Ordovician Pingliang Formation in southern Ordos Basin range from 0.19 to 2.59 with an average of 0.96. The Sr/Ba ratios of the marine mudstones of the lower Permian Liangshan Formation in Dushan area of Guizhou Province range from 0.14 to 2.79 with an average of 0.91. The Sr/Ba ratios of the mudstones of marine-continental transitional facie of Permian Shanxi Formation in Ordos Basin range from 0.13 to 0.89 with an average of 0.36. The Sr/Ba ratios of the mudstones and lime mudstones in the Linxi Formation of the study area range from 0.1 to 3.09 with an average of 0.93. The Sr/Ba ratios of the mudstones and lime

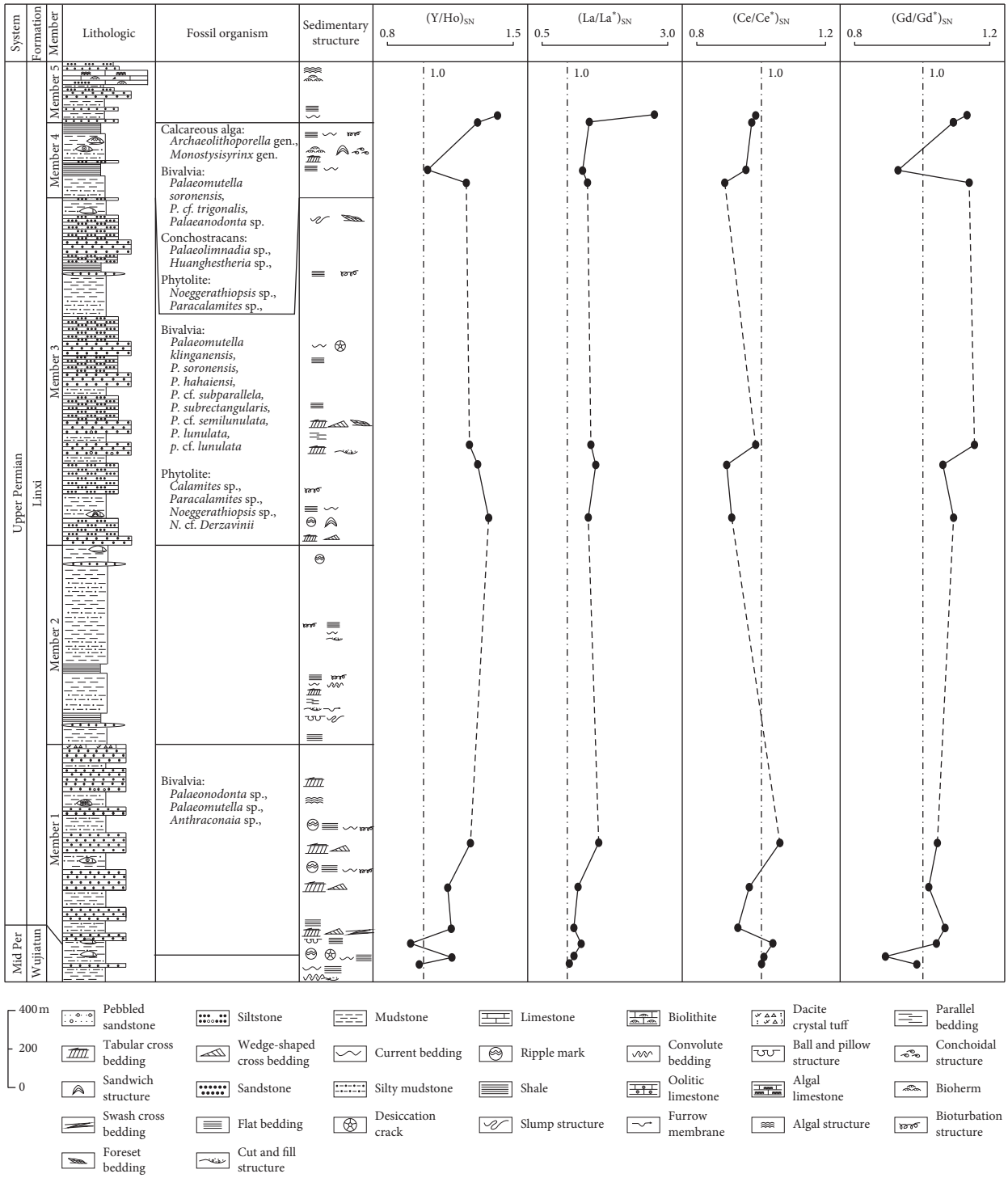

Figure 5: The vertical distribution characteristics of shale-normalised REE + Y of Linxi Formation in the Linxi area.

mudstones of Linxi Formation correspond well with the Sr/Ba ratios of the marine mudstones and the mudstones of marine-continental transitional facie in the other areas of China. The Sr/Ba ratios indicate that the Linxi Formation limestone mainly formed in a salt water environment and develop bathyal sea sedimentary environment or have been affected by terrestrial debris (the Sr/Ba ratios of sample LG 29-1H <0.2).

In addition, B is relatively enriched in marine shales, whereas Ga is relatively enriched in terrestrial shales. Therefore, the B/Ga ratio can be used to distinguish between marine and terrestrial sedimentary environments to a certain degree [36]. Yan et al. conducted a comprehensive study of the Mesozoic biological, mineral, and geochemical characteristics of the Paleocene-Pliocene strata of the Northern Jiangsu basin [39]. Based on a statistical

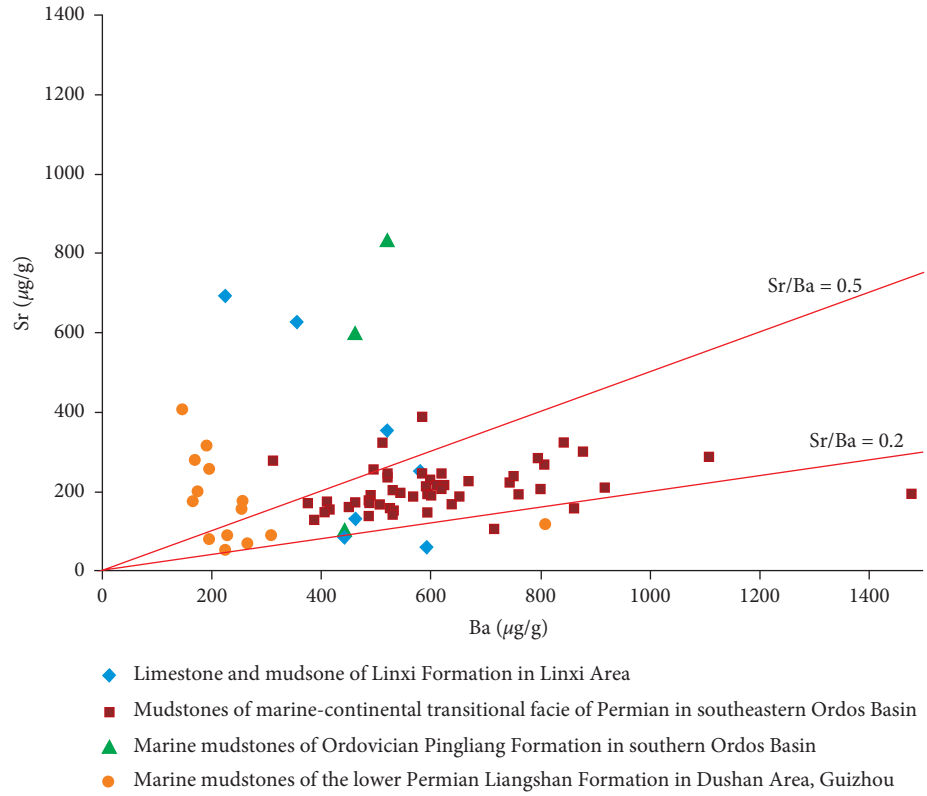

Figure 6: Relationship between the Sr and Ba contents of the Linxi Formation limestone from the Linxi area Guandi profile in eastern Inner Mongolia and comparison with other regions in China.

comparison between ancient American marine sediments, modern marine sediments, ancient terrestrial sediments, modern freshwater sediments, modern Chinese marine sediments, and modern lacustrine sediments, they concluded that the B/Ga ratio of terrestrial sediment is less than 3.3, and ratios greater than 3.3 represent sea-land transitional zones and marine sedimentary environments. To more intuitively contrast the content of B and Ga and assess the deposition environment, the data of B and G contents of shale in different regions of the world have been counted and are presented in Table 5 and shown in Figure 6. The analysis indicates that the B and Ga content of the Changxingjie marine shale in southern China varies from 34.7 μg/g to 141.0 μg/g and from 6.8 μg/g to 25.4 μg/g, respectively, and the average value of B/Ga is 4.79 [40]. The B and Ga content of the Permian terrestrial mudstone in Zhungeer Basins of China varies from 14.2 μg/g to 20.0 μg/g and from 4.4 μg/g to 18.5 μg/g, respectively, and with the average values (B/Ga) of 2.27 [37]. The B and Ga content of the ancient freshwater argillaceous sediments in the United States varies from 8.0 μg/g to 55.0 μg/g and from 9.0 μg/g to 25.0 μg/g, respectively, and with the average values (B/Ga) of 2.02 [41]. The B and Ga content of the ancient marine argillaceous sediment in the United States varies from 65.0 μg/g to 187.0 μg/g and from 10.0 μg/g to 39.0 μg/g, respectively, and with the average values (B/Ga) of 5.77 [41]. The B and Ga content of the inner shelf mudstone off the east coast of Inida varies from 80.0 μg/g to 130.0 μg/g and from 11.0 μg/g to 33.0 μg/g, respectively, and with the average values (B/Ga) of 4.84. The B and Ga content of the outer shelf mudstone off the east coast of Inida varies from 90.0 μg/g to 160.0 μg/g and from 16.0 μg/g to 34.0 μg/g, respectively, and with the average values (B/Ga) of 4.81 [42]. In the study area, the B and Ga content of Linxi Formation mudstone varies from 33.4 μg/g to 150.0 μg/g and from 7.7 μg/g to 22.1 μg/g, respectively. The B/Ga ratios of Linxi Formation mudstone varies from 1.90 to 7.94 with an average of 4.62 being greater than 3.3, except for the mudstone (Sample LG 75-4, B/Ga, 1.9) at the top of section Lin5, and this corresponds well with the marine mudstone from the other area of the world (Figure 7). The relative B and Ga contents of the mudstone from the Linxi Formation indicate a predominantly marine sedimentary environment during deposition of the Linxi Formation and that the formation was affected by terrestrial debris at the end of the deposition of section Lin5.

5.3. Strontium Isotope Distribution and Sedimentary Environment. The stable evolutionary characteristics of Sr isotopes provide a basis for the comparison of Sr isotopes in seawater of the same geological age around the world [43]. In terms of the various sources of Sr, due to the weathering and leaching of crustal Si-Al rocks, lakes, rivers, and groundwater from terrestrial sources transport a large amount of radiogenic ^{87}Sr, which is generated in their catchments (basin), and thus, they have high ^{87}Sr/^{86}Sr values (about 0.7115) [44]. However, seawater transports Sr into the mantle at subduction zones, and Sr enters the seawater at

Table 4: Sr and Ba data of Permian in other areas of China.

Sample	Sr	Ba	Sample	Sr	Ba	Sr	Ba
	124.0	464.5		186.1	652.2	149.8	406.2
	99.7	286.3		285.2	794.3	244.4	519.3
[*1]Marine mudstones of Ordovician Pingliang Formation in Southern Ordos Basin	102.7	543.9		237.6	521.2	187.9	566.6
	273.4	246.6		171.3	486.5	167.9	637.9
	830.1	319.9		324.0	841.8	170.8	374.1
	598.4	471.1		240.1	749.4	230.6	597.0
	70.9	264.0		269.4	807.4	245.8	583.8
	117.0	808.0		206.3	619.7	323.9	510.8
	53.6	224.0		178.4	486.0	217.1	609.0
	90.6	307.0		215.2	624.5	162.8	448.9
	90.3	228.0		299.3	877.5	172.8	460.7
	258.0	194.0	[*3]Mudstones of marine-continental transitional facie of Permian Shanxi Formation in Ordos Basin	225.7	668.1	175.8	409.4
	177.0	164.0		289.0	1108	190.3	600.6
	200.0	173.0		193.2	592.0	192.4	760.8
[*2]Marine mudstones of the lower Permian Liangshan Formation in Dushan area of Guizhou Province, China	157.0	254.0		196.3	544.5	143.2	530.4
	280.0	168.0		202.2	529.4	277.4	310.2
	80.6	195.0		222.3	742.9	150.5	531.4
	316.0	190.0		247.1	619.4	159.3	860.1
	408.0	146.0		256.3	495.2	194.9	1478
	176.9	255.0		138.9	486.1	130.0	386.7
				105.1	714.9	211.1	917.5
				211.8	589.7	148.1	593.4
				155.1	414.8	158.3	526.0
				190.8	489.2	166.9	505.5
				388.7	583.2	207.3	799.3

[*1]Data from Ni et al. [37]; [*2]data from Zhang et al. [38]; [*3]data from Chen et al. [34].

Table 5: B and Ga data of argillaceous sediments in the other places of the world.

Sample	B	Ga	Sample	B	Ga	Sample	B	Ga	Sample	B	Ga
Mudstone of Permian in Chao County[*1]	95.7	22.1	Ancient marine argillaceous sediments, United States[*3]	95	30	The inner shelf mudstone off the East Coast of Inida[*4]	120	33	The outer shelf mudstone off the East Coast of Inida[*6]	160	32
	97.8	20.4		106	29		80	19		160	34
	57.3	20.3		69	18		100	25		110	25
	49.8	20.0		164	25		110	33		110	24
	52.5	22.2		166	18		110	22		100	16
	37	12		178	31		90	11		100	23
	32	12		87	26		86	20		100	22
	18	12		111	38		120	25		100	21
	8	10		142	39		86	20		130	27
	54	17		179	38		110	25		100	20
Ancient fresh-water argillaceous sediments, United States[*2]	34	20		120	28		80	17		120	27
	10	9		187	15		130	28		110	22
	26	15		127	20		100	20		90	20
	55	25		177	22		130	18		110	27
	26	19		65	10	Terrestrial mudstone of Permian in Junggar Basin[*5]	14.22	4.41		130	23
	52	18		122	20		29.14	18.53			
				179	20		20.00	9.93			
				74	17						

[*1]Data from Cheng [40]; [*2,*3]data from Potter et al. [41]; [*4,*6]data from Rao and Rao [42]; [*5]data from Zhang et al. [37].

midoceanic ridge hydrothermal systems [45]. The seawater also interacts with terrestrial waters that drain into the oceans, resulting in the $^{87}Sr/^{86}Sr$ values of modern seawater being approximately 0.7092 [46]. Carbonates and some fossils can record the composition of Sr isotopes in sedimentary media. The composition and evolution of Sr isotopes ($^{87}Sr/^{86}Sr$ values) throughout geologic history have been well documented and reported. Therefore, by comparing the Sr isotopic compositions of endogenous carbonate rocks that have not been altered to the Sr isotopic composition of seawater during that geologic period, we can determine whether the sedimentary strata was deposited in a marine sedimentary environment or a terrestrial sedimentary environment. As shown in Figure 7, Korte et al. established the background value (0.7073–0.7074) of $^{87}Sr/^{86}Sr$ during the Permian and the Triassic by the analysis of Sr

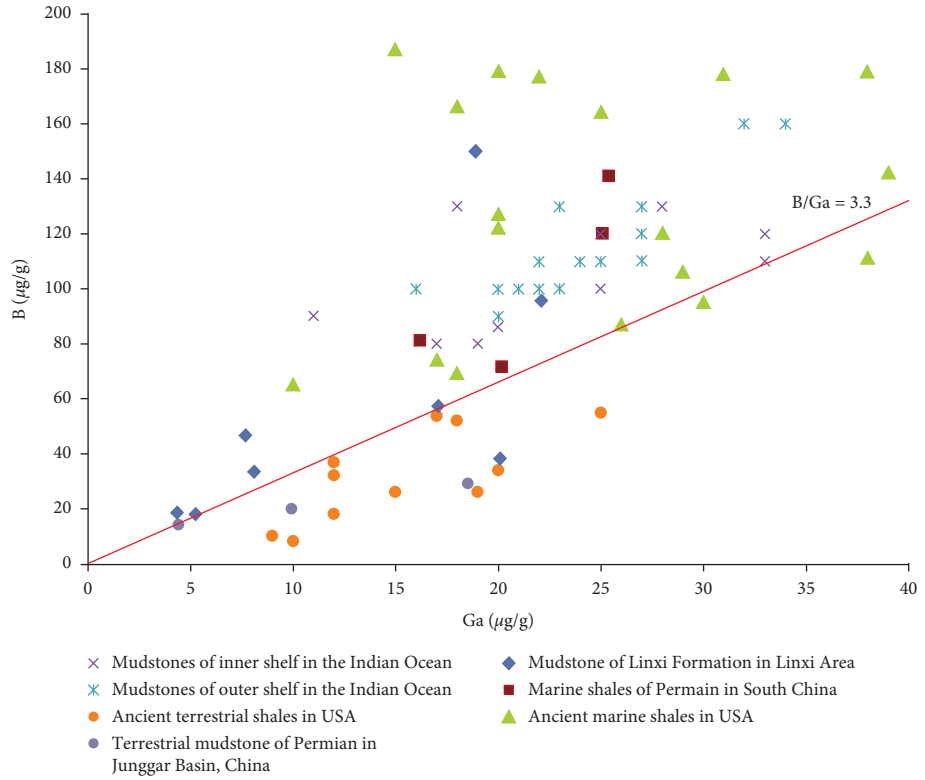

FIGURE 7: Relationship between the B and Ga contents of the Linxi Formation mudstone from the Linxi area Guandi profile in eastern Inner Mongolia and comparison with other regions of the world.

isotopes from brachiopods [9, 10, 28]. Tian and Zheng found that $^{87}Sr/^{86}Sr$ values of Permian marine limestone range from 0.7072 to 0.7077 in South China [8]. Huang et al. found that $^{87}Sr/^{86}Sr$ values of the Late Permian seawater range from 0.7067 to 0.7076 by analyzing the Sr isotopes of marine carbonate rocks from the Upper Permian in the Upper Yangtze region [11]. Martin and Macdougall researched the contents of Sr isotopes in conodonts of Permian/Triassic from the United States and Pakistan, and they found that $^{87}Sr/^{86}Sr$ values of seawater in Permian/Triassic range from 0.7069 to 0.7089 (Table 2) [12]. The results of Sr isotopic analysis show that the $^{87}Sr/^{86}Sr$ values of the Linxi Formation limestone in the Linxi Guandi profile range from 0.70728 to 0.70795 and distribute within the range of Sr isotope composition of Permian seawater (Figure 8). The $^{87}Sr/^{86}Sr$ values of the four limestone from section Lin1 to the bottom of section Lin3 range from 0.70753 to 0.70776 and fall within the Sr isotope range of the Late Permian Wujiaping and Changxing Period marine carbonates in southern China, indicating a shallow water carbonate sedimentary environment. The $^{87}Sr/^{86}Sr$ values of five limestone samples from sections Lin4 and Lin5 range from 0.70729 to 0.70795. Comparing with the contents of Sr isotope of the Permian marine limestone in other area of China, the $^{87}Sr/^{86}Sr$ values of the lower and upper limestone of section Lin4 have abnormally high values of 0.70795 and 0.70780, respectively, reflecting the fact that terrestrial water or terrestrial debris mixed with the main sediment supply. In addition, the $^{87}Sr/^{86}Sr$ values of one limestone sample each (sample numbers LG72-13T and LG73-2CT) from the top of section Lin4 and the bottom of section Lin5 are consistent with the $^{87}Sr/^{86}Sr$ background values (0.7073–0.7074) of the global Late Permian paleocean and exhibit relatively low $^{87}Sr/^{86}Sr$ values. The interpretation of this phenomenon is that the upper part of the Linxi Formation was deposited during a stage of rift closing and uplift accompanied by intense volcanic eruptions. The eruptions of magmas from a mantle source affected the composition of the Sr isotopes, which resulted in a decrease in the $^{87}Sr/^{86}Sr$ value of the sediments. The tuff interlayer in section Lin5 also supports the occurrence of volcanic activity.

5.4. C Isotope Distribution and Sedimentary Environment. The compositions of carbon isotopes in carbonate rocks and their changes can effectively trace sedimentary environments, diagenetic environments, and other geological processes [14, 47–52]. The $\delta^{13}C$ values of all nine limestone samples in the Linxi Formation range from −4.0‰ to 2.4‰ with a variation range of 6.4‰, and 67% of them are in the range of $\delta^{13}C$ values (0 ± 2‰) of normal seawater, indicating a normal marine sedimentary environment in the Linxi area. Compared with the $\delta^{13}C$ of marine Permian carbonate rocks (e.g., eastern Inner Mongolia, Changxing District of Zhejiang and Khorat Basin of Thailand) and Triassic lacustrine limestone in Linxi area (Table 3), the $\delta^{13}C$ values of limestone in the Linxi Formation are in the range of marine limestone but significantly higher than those of the

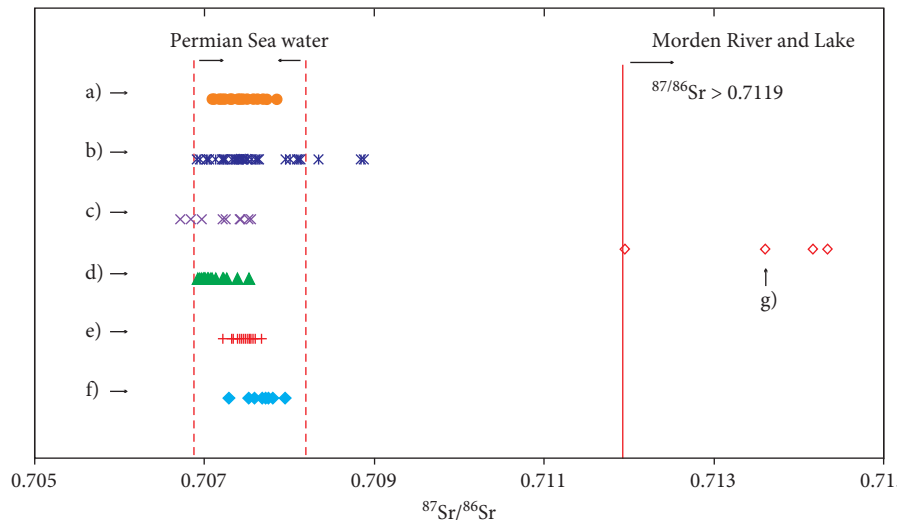

Figure 8: Sr isotopic compositions of the Linxi Formation limestone from the Linxi area Guandi profile in eastern Inner Mongolia and the comparison with the $^{87}Sr/^{86}Sr$ values of Permian in the other area: the Sr isotopic compositions of (a) conodonts during the Permian and the Triassic in Pakistan [12], (b) conodonts during the Permian and the Triassic in the United States [12], (c) marine carbonates rocks of Late Permian in Upper Yangtze region [11], (d) conodonts during the Permian and the Triassic in Abadeh, Iran [9, 10], (e) marine limestone of Permian in South China [8], (f) Permian Linxi Formation limestone from the Linxi area in eastern Inner Mongolia, and (g) the lacustrine limestone of Triassic from the Linxi area in eastern Inner Mongolia.

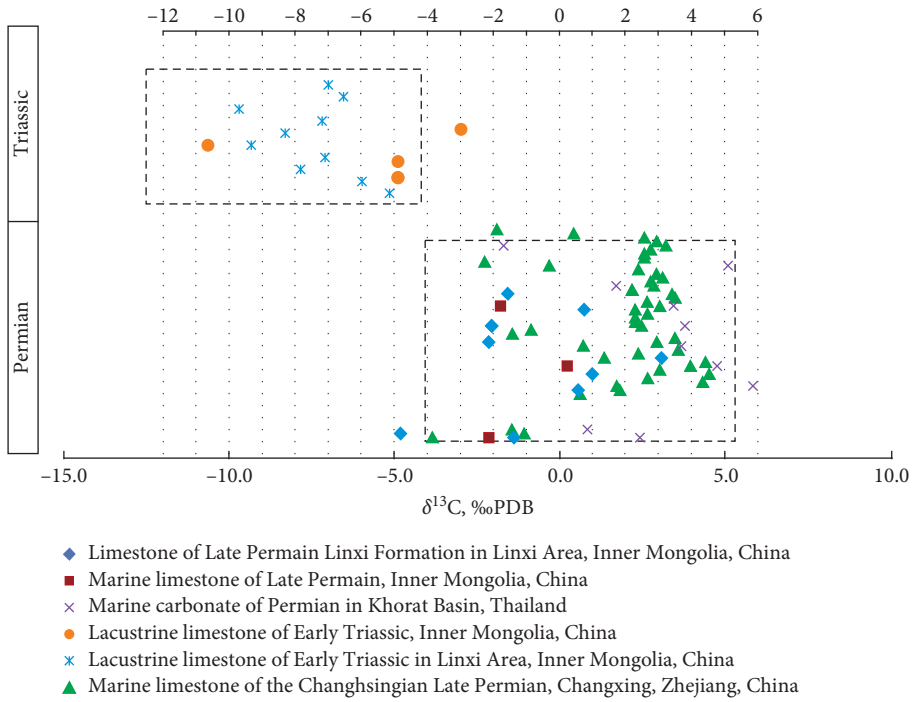

Figure 9: C isotopic compositions of the Linxi Formation limestone and the lacustrine limestone (Triassic) from the Linxi area in eastern Inner Mongolia and the comparison with the C isotopic of marine limestone (Permian) in the other areas of the world.

lacustrine limestone (Figure 9). However, it should be noted that individual sample with a low $\delta^{13}C$ value indicates a further differentiation in the sedimentary environment under normal marine background. For instance, the difference of seawater circulation, atmospheric circulation, and the accordingly production rate of organic carbon may cause changes in carbon isotope composition in limestone. The extensive development of plant debris and bioturbation structures in the Linxi mudstone indicate a shallow water environment with sufficient biomass during the deposition period of the Late Permian Linxi Formation. And so, we infer that the ^{12}C produced by the biological respiration, the oxidation of organic matter, and the freshwater recharge of low-carbon isotopic compositions all contribute to the low

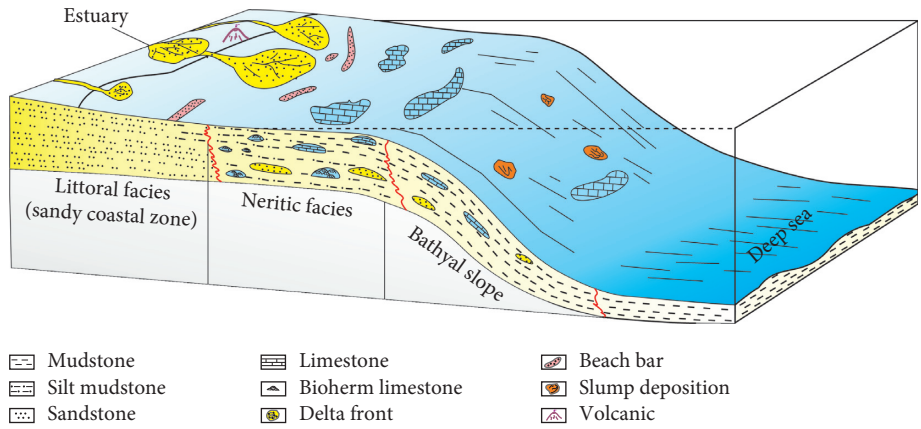

Figure 10: Sedimentary model of the Late Permian Linxi Formation in the Linxi area of eastern Inner Mongolia.

carbon isotope value of diagenetic fluids. Moreover, frequent volcanic activity was triggered by strong tectonics at the Late Permian in the study area and the volcanism produced a lot of CO_2. The carbon isotopic compositions of CO_2 (−5‰) may also be one of the reasons for the lower $\delta^{13}C$ value of limestone in the study area.

5.5. Sedimentary Environment and Its Evolution. These features of trace elements, isotopes, and sedimentary characteristics indicate that the environment of Linxi Formation is closed to the element and isotope compositions characteristic of littoral facies and neritic facies but with freshwater inputs from continental weathering.

Although the characteristics of limestone or shale of Linxi Formation yielded very consistent results, significant differences can be noted between 5 sections of Linxi Formation (Lin1–5) (Figures 5–9). Through the minor differences of trace compositions, lithologic association, sedimentary structures, and paleontology fossils of the Linxi Formation, we made the sedimentary environment dividing in detail. The lithology of section Lin1 of the Linxi Formation is mainly composed of sandy and silty sediments that exhibit symmetrical ripple bedding, horizontal bedding, and other sedimentary structures with directional significance for hydrodynamic conditions. The limestones at the lower section of Lin1 display a slight positive La anomaly, lack of Ce, Gd, and Y anomaly, and the upper section evolves into the characteristic of distinct positive La anomaly and slight positive Y anomaly. These distribution features of REE combining with Sr-C isotope and trace element indicate that the sedimentary environment of section Lin1 evolved from the proximal section of littoral facies with terrigenous clastic mixing to the distal section of littoral facies. Compare with the Lin1 section, the mud content of section Lin2 increased obviously which composed of mudstone, silt mudstone, and shale. The lower part of section Lin2 exhibited slump structures, convolute bedding, and flat bedding; the upper parts developed flat bedding, bioturbation structures, ripple mark structures, and current bedding. These sedimentary structures combining with the distribution of Sr-C isotope and Sr/Ba and B/Ga ratio indicate that the water body deepens during the depositional phase of section Lin2, and the sedimentary environments are interpreted to be bathyal slope to neritic facies. The sandstone content of the section Lin3 increases relatively. The lower parts of section Lin3 exhibited tabular cross bedding, wedge-shaped cross bedding, flat bedding, and ripple mark structures, and these sedimentary structures combining with the distributions of REE, C isotope, and Sr/Ba ratios of the limestones indicated that the sedimentary environment was close to the distal section of littoral facies. The middle and upper parts of section Lin3 developed foreset bedding, desiccation crack, bioturbation structure, slump structure, and current bedding, which indicated the sedimentary environment of delta front and littoral facies. The section Lin4 mainly composed of shale, silty mudstone, argillaceous siltstones, and limestone lenses. The geochemical characteristics of limestones with lower $^{87}Sr/^{86}Sr$ values, slight positive La and Y anomaly, and the sedimentary structures composing of flat bedding, tabular cross bedding, current bedding, bioturbation structure, and the typical marine fossils observed in this section indicate that the sedimentary environment of section Lin4 is mainly neritic facies. Section Lin5 is composed of sandstones and bioherm limestones and develops bryozoans and sponge bone fossils. The geochemical characteristics of the limestones in section Lin5 display a marine distribution pattern, which is displaying as low $^{87}Sr/^{86}Sr$ values and distinct positive La and Y anomaly. Combined with the sedimentary and geochemical characteristics, the sedimentary environment of section Lin5 is interpreted to be neritic facies.

6. Conclusions

The lithologic association of the Linxi Formation is mainly composed of clastic rocks, with interbedded carbonates and lenticular limestone bodies. The upper and lower units of the Linxi Formation limestones consistently show initial $\delta^{13}C$ values, $^{87}Sr/^{86}Sr$ ratios, and the similar REE + Y patterns that are characterized by depletion of LREE relative to HREE, distinct positive La anomaly, minor positive Y anomaly, weak positive Gd anomaly, lack of Ce anomaly, and the same range of Sr/Ba and B/Ga ratio. In general, the sedimentary

environment of the Linxi Formation of Late Permian is still dominated by an open marine environment and has freshwater inputs from continental weathering. The marine environments can be divided into 3 major types which are littoral facies, neritic facies, and bathyal facies (Figure 10). In addition, due to the regional uplift and the accompanying shallow water environment, a delta front environment of sea-land transition zone sediments also developed in the study area in addition to the marine sedimentary environment. The sedimentary environment of the Late Permian Linxi Formation underwent a process from littoral facies to neritic facies (bathyal facies) and then through littoral facies, delta front to neritic facies.

Data Availability

The raw data used to support the findings of this study are available from the corresponding author upon request.

Conflicts of Interest

The authors declare that they have no conflicts of interest.

Acknowledgments

This research was partially supported by the National Key R & D Program of China under grant 2017YFC0603103 and the National Natural Science Foundation of China (no. 41572098).

References

[1] Z. J. He, S. W. Liu, J. S. Ren, and Y. Wang, "Late Permian-early Triassic sedimentary evolution and tectonic setting of the Linxi region, inner Mongolia," *Regional Geology of China*, vol. 16, no. 4, pp. 403–409, 1997.

[2] Y. Zhang, S. Tian, Z. Li et al., "Discovery of marine fossils in the upper part of the Permian Linxi formation in Lopingian, Xingmeng area, China," *Chinese Science Bulletin*, vol. 59, no. 1, pp. 62–74, 2014.

[3] S. Tian, Z. Li, Y. Zhang, Y. Gong, D. Zhai, and M. Wang, "Late carboniferous-Permian tectono-geographical conditions and development in Eastern Inner Mengolia and adjacent areas," *Acta Geologica Sinica*, vol. 90, no. 4, pp. 688–707, 2016.

[4] H. Yu, "Sedimentary facies and palaeogeography of the Songliao Basin and its peripheral areas during Carboniferous-Permian time," *Sedimentary Geology and Tethyan Geology*, vol. 21, no. 4, pp. 70–83, 2001.

[5] D. Q. Fang, J. B. Yun, Q. S. Pang, L. H. Zhao, and R. Zhao, "Discussion of carboniferous in the periphery of Songliao Basin," *Journal of Daqing Petroleum Institute*, vol. 28, no. 4, pp. 93–95, 2004.

[6] R. Zhu, H. Xu, S. Deng, and H. Guo, "Lithofacies palaeogeography of the Permian in northern China," *Journal of Palaeogeography*, vol. 9, no. 2, pp. 133–142, 2007.

[7] S. G. Tian, Z. S. Li, J. T. Wang, L. P. Zhang, and S. W. Niu, "Carboniferous-Permian tectonic and stratigraphic framework of eastern Inner Mongolia as well as adjacent areas and its formation environment," *Geological Bulletin of China*, vol. 31, no. 10, pp. 1554–1564, 2012.

[8] J. Tian and Y. Zheng, "The revolution of the isotopic composition of strontium in the Permian Paleo-ocean in South China," *Acta Sedimentologica Sinica*, vol. 13, no. 4, pp. 125–130, 1995.

[9] C. Korte, H. W. Kozur, M. M. Joachimski, H. Strauss, J. Veizer, and L. Schwark, "Carbon, sulfur, oxygen and strontium isotope records, organic geochemistry and biostratigraphy across the Permian/Triassic boundary in Abadeh, Iran," *International Journal of Earth Sciences*, vol. 93, no. 4, pp. 565–581, 2004.

[10] C. Korte, T. Jasper, H. W. Kozur, and J. Veizer, "$^{87}Sr/^{86}Sr$ record of Permian seawater," *Palaeogeography Palaeoclimatology Palaeoecology*, vol. 240, no. 1-2, pp. 89–107, 2006.

[11] S. J. Huang, H. Shi, M. Zhang, L. C. Shen, J. Liu, and W. H. Wu, "Strontium isotope evolution and global sea–level changes of Carboniferous and Permian Marine carbonate, Upper Yangtze Platform," *Acta Sedimentologica Sinica*, vol. 19, no. 4, pp. 481–487, 2001.

[12] E. E. Martin and J. D. Macdougall, "Sr and Nd isotopes at the Permian/Triassic boundary: a record of climate change," *Chemical Geology*, vol. 125, no. 1-2, pp. 73–99, 1995.

[13] G. C. Du, H. Cang, S. Q. Hu, Q. R. Cao, and P. P. Gao, "Geochemical characteristics and its paleo-environmental significance of Permian carbonate rocks in Khorat Basin, Thailand," *Global Geology*, vol. 36, no. 1, pp. 135–143, 2017.

[14] Y. Li, "Carbon and oxygen isotope stratigraphy of the upper Permian changhsingian limestone in meishan section D, changxing, Zhejiang," *Journal of Stratigraphy*, vol. 22, no. 1, pp. 36–41, 1998.

[15] J. Ryu, A. D. Jacobson, C. Holmden, C. Lundstrom, and Z. Zhang, "The major ion, $\delta^{44/40}$ca, $\delta^{44/42}$ca, and $\delta^{26/24}$mg geochemistry of granite weathering at ph = 1 and t = 25°C: power-law processes and the relative reactivity of minerals," *Geochimica Et Cosmochimica Acta*, vol. 75, no. 20, pp. 6004–6026, 2016.

[16] S. R. Taylor and S. M. Mclennan, "The geochemical evolution of the continental crust," *Reviews of Geophysics*, vol. 33, no. 2, pp. 241–265, 1995.

[17] J. Zhang and Y. Nozaki, "Rare earth elements and yttrium in seawater: ICP-MS determinations in the east caroline, coral sea, and south Fiji basins of the western south Pacific ocean," *Geochimica Et Cosmochimica Acta*, vol. 60, no. 23, pp. 4631–4644, 1996.

[18] C. R. German, B. P. Holliday, and H. Elderfield, "Redox cycling of rare earth elements in the suboxic zone of the Black Sea," *Geochimica Et Cosmochimica Acta*, vol. 55, no. 12, pp. 3553–3558, 1991.

[19] Y. Nozaki, D. Lerche, D. S. Alibo, and A. Snidvongs, "The estuarine geochemistry of rare earth elements and indium in the Chao Phraya River, Thailand," *Geochimica Et Cosmochimica Acta*, vol. 64, no. 23, pp. 3983–3994, 2000.

[20] T. Liang, L. Wang, C. Zhang, L. Ding, S. Ding, and X. Yan, "Contents and their distribution pattern of rare earth elements in water and sediment of intertidalite," *Journal of the Chinese Rare Earth Society*, vol. 23, no. 1, pp. 68–74, 2005.

[21] R. Bolhar and M. Vankranendonk, "A non-marine depositional setting for the northern Fortescue Group, Pilbara Craton, inferred from trace element geochemistry of stromatolitic carbonates," *Precambrian Research*, vol. 155, no. 3-4, pp. 229–250, 2007.

[22] M. J. V. Kranendonk, G. E. Webb, and B. S. Kamber, "Geological and trace element evidence for a marine sedimentary environment of deposition and biogenicity of 3.45 Ga stromatolitic carbonates in the Pilbara Craton, and

support for a reducing Archaean ocean," *Geobiology*, vol. 1, no. 2, pp. 91–108, 2003.

[23] M. Bau and P. Dulski, "Comparing yttrium and rare earths in hydrothermal fluids from the Mid-Atlantic Ridge: implications for Y and REE behaviour during near-vent mixing and for the Y/Ho ratio of Proterozoic seawater," *Chemical Geology*, vol. 155, no. 1-2, pp. 77–90, 1999.

[24] S. B. Ojiambo, W. B. Lyons, K. A. Welch, R. J. Poreda, and K. H. Johannesson, "Strontium isotopes and rare earth elements as tracers of groundwater–lake water interactions, Lake Naivasha, Kenya," *Applied Geochemistry*, vol. 18, no. 11, pp. 1789–1805, 2003.

[25] Z. Z. Zhu, Z. L. Wang, B. Gao, and S. L. Wang, "Geochemical characteristics of rare earth elements in Lake Chaohu, East China," *Geochimica*, vol. 35, no. 6, pp. 639–644, 2006.

[26] H. E. Frimmel, "Trace element distribution in Neoproterozoic carbonates as palaeoenvironmental indicator," *Chemical Geology*, vol. 258, no. 3-4, pp. 338–353, 2009.

[27] A. J. Kaufman, S. B. Jacobsen, and A. H. Knoll, "The Vendian record of Sr and C isotopic variations in seawater: implications for tectonics and paleoclimate," *Earth and Planetary Science Letters*, vol. 120, no. 3-4, pp. 409–430, 1993.

[28] C. Korte, H. W. Kozur, P. Bruckschen, and J. Veizer, "Strontium isotope evolution of late Permian and Triassic seawater," *Geochimica et Cosmochimica Acta*, vol. 67, no. 1, pp. 47–62, 2003.

[29] G. E. Webb and B. S. Kamber, "Rare earth elements in Holocene reefal microbialites: a new shallow seawater proxy," *Geochimica Et Cosmochimica Acta*, vol. 64, no. 9, pp. 1557–1565, 2000.

[30] R. Bolhar, B. S. Kamber, S. Moorbath, C. M. Fedo, and M. J. Whitehouse, "Characterisation of early archaean chemical sediments by trace element signatures," *Earth and Planetary Science Letters*, vol. 222, no. 1, pp. 43–60, 2004.

[31] G. A. Shields and G. E. Webb, "Has the REE composition of seawater changed over geological time?" *Chemical Geology*, vol. 204, no. 1-2, pp. 103–107, 2004.

[32] H. E. Frimmel, "Trace element distribution in Neoproterozoic carbonates as palaeoenvironmental indicator," *Chemical Geology*, vol. 258, no. 3-4, pp. 338–353, 2009.

[33] Z. X. Ma, B. Li, X. T. Liu, and L. Luo, "Geochemical characteristics and implications for the evolution of sedimentary environments of early cambrian Qingxudong Formation in eastern Guizhou, Southwestern China," *Geological Science & Technology Information*, vol. 34, no. 2, pp. 71–77, 2015.

[34] H. D. Chen, L. I. Jie, and C. G. Zhang, "Discussion of sedimentary environment and its geological enlightenment of Shanxi Formation in Ordos Basin," *Acta Petrologica Sinica*, vol. 27, no. 8, pp. 2213–2229, 2011.

[35] N. Adachi, Y. Ezaki, and J. Liu, "The late early cambrian microbial reefs immediately after the demise of archaeocyathan reefs, Hunan Province, South China," *Palaeogeography, Palaeoclimatology, Palaeoecology*, vol. 407, no. 4, pp. 45–55, 2014.

[36] W. Wei and T. J. Algeo, "Elemental proxies for paleosalinity analysis of ancient shales and mudrocks," *Geochimica et Cosmochimica Acta*, In press, 2019.

[37] G. W Zhang, S. Tao, D. Z. Tang, Y. B. Xu, Y. Cui, and Q. Wang, "Geochemical characteristics of trace elements and rare earth elements in Permian Lucaogou oil shale, Santanghu Basin," *Journal of China Coal Society*, vol. 42, no. 8, pp. 2081–2089.

[38] G. T. Zhang, Z. Q. Peng, C. S. Wang, and Z. H. Li, "Geochemical characteristics of the lower Permian Liangshan Formation in Dushan area of Guizhou Province and their implications for the paleoenvironment," *Geology in China*, vol. 43, no. 4, pp. 1291–1303, 2016.

[39] Q. Yan, G. Zhang, L. Xiang et al., "Marine inundation and related sedimentary environment of Funing group (lower Paleogene), in Jinhu depression, North Jiangsu Plain," *Acta Geological Sinica*, vol. 1, pp. 74–84, 1979.

[40] A. Cheng, "Content of B and B/Ga ratio of the Yingying Formation in Chao County, Anhui Province," *Journal of Stratigraphy*, vol. 18, no. 4, pp. 299-300, 1994.

[41] P. E. Potter, N. F. Shimp, and J. Witters, "Trace elements in marine and fresh-water argillaceous sediments," *Geochimica Et Cosmochimica Acta*, vol. 27, no. 6, pp. 669–694, 1963.

[42] N. V. N. D. Rao and M. P. Rao, "Trace-element distribution in the continental-shelf sediments off the east coast of India," *Marine Geology*, vol. 15, no. 3, pp. 43–48, 1973.

[43] C. E. Jones, "Seawater strontium isotopes, oceanic anoxic events, and seafloor hydrothermal activity in the Jurassic and Cretaceous," *American Journal of Science*, vol. 301, no. 2, pp. 112–149, 2001.

[44] B. E. Crowley, J. H. Miller, and C. P. Bataille, "Strontium isotopes ($^{87}Sr/^{86}Sr$) in terrestrial ecological and palaeoecological research: empirical efforts and recent advances in continental-scale models," *Biological Reviews*, vol. 92, no. 1, pp. 43–59, 2017.

[45] M. Harris, R. M. Coggon, C. E. Smith-Duque, M. J. Cooper, J. A. Teagle, and D. A. H. Damon, "Channelling of hydrothermal fluids during the accretion and evolution of the upper oceanic crust: Sr isotope evidence from ODP Hole 1256D," *Earth and Planetary Science Letters*, vol. 416, pp. 56–66, 2015.

[46] J. M. McArthur, "Recent trends in strontium isotope stratigraphy," *Terra Nova*, vol. 6, no. 4, pp. 331–358, 2010.

[47] D. Reghellin, H. K. Coxall, G. R. Dickens, and J. Backman, "Carbon and oxygen isotopes of bulk carbonate in sediment deposited beneath the eastern equatorial Pacific over the last 8 million years," *Paleoceanography*, vol. 30, no. 10, pp. 1261–1286, 2016.

[48] X. Li, W. Xu, W. Liu et al., "Climatic and environmental indications of carbon and oxygen isotopes from the Lower Cretaceous calcrete and lacustrine carbonates in Southeast and Northwest China," *Palaeogeography, Palaeoclimatology, Palaeoecology*, vol. 385, no. 3, pp. 171–189, 2013.

[49] M. M. Vieira, A. N. Sial, L. F. De Ros, and S. Morad, "Origin of holocene beachrock cements in Northeastern Brazil: evidence from carbon and oxygen isotopes," *Journal of South American Earth Sciences*, vol. 79, pp. 401–408, 2017.

[50] B. Banerjee, S. M. Ahmad, W. Raza, and T. Raza, "Paleoceanographic changes in the Northeast Indian Ocean during middle Miocene inferred from carbon and oxygen isotopes of foraminiferal fossil shells," *Palaeogeography, Palaeoclimatology, Palaeoecology*, vol. 466, pp. 166–173, 2017.

[51] Q. Zhang, B. Liang, F. Qin, J. Cao, D. Yong, and J. Li, "Environmental and geochemical significance of carbon and oxygen isotopes of Ordovician carbonate paleokarst in Lunnan, Tarim Basin," *Environmental Earth Sciences*, vol. 75, no. 14, pp. 1–11, 2016.

[52] D. X. Zhai, Y. S. Zhang, S. G. Tian et al., "The late Permian sedimentary environments of Linxi formation in Xingmeng area: constraints from carbon and oxygen isotopes and trace elements," *Acta Geoscientica Sinica*, vol. 36, no. 3, pp. 333–343, 2015.